QUARTERLY OF APPLIED MATHEMATICS
VOLUME XLIV, NUMBER 4
JANUARY 1987, PAGES 757-772

ISOCHROMATIC LINES AND DYNAMIC PUNCHING OF A STRESSED ELASTIC PLATE*

BY

D. W. BARCLAY (*University of New Brunswick, Canada*)

AND

R. J. TAIT AND T. B. MOODIE (*University of Alberta, Canada*)

Abstract. Diagrams of the developing isochromatic curve patterns associated with the dynamic stress field of a normally impacted isotropic plate under uniaxial tension are computed to show the accompanying wave fronts and zones of stress when plugging occurs.

1. Introduction. In this paper we consider the evolution in time of the isochromatic lines for the stress field in an isotropic plate subject to uniform uniaxial tension and impacted normally by a flat-nosed cylindrical projectile. We assume that "plugging" occurs. That is, a circular plug of material of approximately the same diameter as the projectile is removed from the plate; and unloading waves emanate from the circular hole.

The problem of determining the stress field has been investigated in [1] and a more detailed description may be found there. An overall view of the stress field is not available, however. In the present paper we have computed the isochromatic lines for the problem at a sequence of time intervals. These lines, of course, correspond to the fringe patterns of photoelasticity.

2. Equations. We follow the notation of [1] here. Given an unbounded isotropic elastic plate, thickness h, in an initial state of uniform uniaxial stress, we have

$$\begin{aligned} \sigma_r &= \tfrac{1}{2}S(1 - \cos(2\theta)), \\ \sigma_\theta &= \tfrac{1}{2}S(1 + \cos(2\theta)), \\ \tau_{r\theta} &= \tfrac{1}{2}S\sin(2\theta), \end{aligned} \tag{2.1}$$

where r, θ are plane polar coordinates, S is a constant, and σ_r, σ_θ, $\tau_{r\theta}$ are the radial, circumferential, and shear components of generalized plane stress. At $t = 0$ a flat-nosed projectile, travelling along the z-axis, begins to punch out a hole of radius $a \gg h$ in the

* Received September 9, 1985.

plate. The boundary conditions at the hole are then taken to be

$$\begin{bmatrix} \sigma_r \\ \tau_{r\theta} \end{bmatrix}_{r=a} = \frac{S}{2}\begin{bmatrix} 1 - \cos(2\theta) \\ \sin(2\theta) \end{bmatrix}\left(1 - \frac{tH(t)}{t^*}\right)H(t^* - t), \tag{2.2}$$

where $H(\cdot)$ denotes the Heaviside step function and t^* is the punching time, which according to [2] is

$$t^* = 2h/w, \tag{2.3}$$

where w is the punch velocity. The situation is illustrated in Fig. 1 of [1].

It is convenient in the following to subtract out the initial stress field and take

$$\begin{bmatrix} \sigma_r \\ \tau_{r\theta} \end{bmatrix}_{r=a} = \frac{S}{2}\begin{bmatrix} 1 - \cos(2\theta) \\ \sin(2\theta) \end{bmatrix}\left[\left(1 - \frac{tH(t)}{t^*}\right)H(t^* - t) - 1\right] \tag{2.4}$$

as our condition at the hole.

For $t > 0$, the equations of motion are

$$\begin{aligned} \frac{\partial \sigma_r}{\partial r} + \frac{1}{r}\frac{\partial \tau_{r\theta}}{\partial \theta} + \frac{\sigma_r - \sigma_\theta}{r} &= \rho \frac{\partial^2 u}{\partial t^2}, \\ \frac{1}{r}\frac{\partial \sigma_\theta}{\partial \theta} + \frac{\partial \tau_{r\theta}}{\partial r} + \frac{2}{r}\tau_{r\theta} &= \rho \frac{\partial^2 v}{\partial t^2}, \end{aligned} \tag{2.5}$$

where ρ is the plate density and u and v are the radial and circumferential components of displacement, respectively. In addition,

$$\begin{aligned} \sigma_r &= \frac{E}{1 - \nu^2}\left[\frac{\partial u}{\partial r} + \nu\left(\frac{u}{r} + \frac{1}{r}\frac{\partial v}{\partial \theta}\right)\right], \\ \sigma_\theta &= \frac{E}{1 - \nu^2}\left[\frac{u}{r} + \frac{1}{r}\frac{\partial v}{\partial \theta} + \nu\frac{\partial u}{\partial r}\right], \\ \tau_{r\theta} &= \mu\left[\frac{1}{r}\frac{\partial u}{\partial \theta} + \frac{\partial v}{\partial r} - \frac{v}{r}\right], \end{aligned} \tag{2.6}$$

where E denotes the Young's modulus, ν the Poisson ratio, and μ the shear modulus for the plate. In addition, we require the quantity

$$\tau_{\max} = \sqrt{\left(\frac{\sigma_r - \sigma_\theta}{2}\right)^2 + \tau_{r\theta}^2}. \tag{2.7}$$

If we introduce the longitudinal and transverse wave speeds c_1, c_2 respectively as

$$c_1^2 = E/\rho(1 - \nu^2), \qquad c_2^2 = \mu/\rho, \tag{2.8}$$

we may nondimensionalize the relevant quantities as

$$\begin{gathered} (\hat{\sigma}_r, \hat{\sigma}_\theta, \hat{\tau}_{r\theta}, \hat{\tau}_{\max}) = (\sigma_r, \sigma_\theta, \tau_{r\theta}, \tau_{\max})/\mu, \\ (\hat{u}, \hat{v}) = (u, v)/a, \qquad \hat{r} = r/a, \qquad \hat{t} = c_2 t/a, \\ \hat{t}^* = c_2 t^*/a, \qquad \hat{c}_1 = c_1/c_2, \qquad \hat{c}_2 = 1, \qquad \hat{S} = S/\mu, \qquad \hat{a} = 1. \end{gathered} \tag{2.9}$$

We assume that in the following, equations (2.1)–(2.7) have been rewritten in nondimensional form using (2.9) and that for convenience the carets have been dropped. In addition, we assume quiescent initial conditions.

3. Solution of the problem. The boundary value problem described in Sec. 2 by Eqs. (2.4)–(2.6) in nondimensional form has been solved in [1] by means of the Laplace transform. If

$$\bar{f}(p) \equiv L\{f(t)\} \equiv \int_0^\infty e^{-pt} f(t)\, dt \tag{3.1}$$

denotes the Laplace transform of $f(t)$, then [1] gives

$$\bar{\tau}_{r\theta} = \left[-2A_2(p)\alpha_2(p,r) + D_2(p)\beta_2(p,r)\right] \sin 2\theta, \tag{3.1}$$

$$\bar{\sigma}_r = A_0(p)\gamma_0(p,r) + \left[A_2(p)\gamma_2(p,r) + 2D_2(p)\delta_2(p,r)\right] \cos 2\theta, \tag{3.2}$$

$$\bar{\sigma}_\theta = (1+\nu)p^2\left[A_0(p)K_0(pr/c_1) + A_2(p)K_2(pr/c_1)\cos 2\theta\right] - \bar{\sigma}_r, \tag{3.3}$$

where

$$A_0(p) = SI/2\gamma_0(p,1), \tag{3.4}$$

$$A_2(p) = -\frac{SI}{2} \cdot \frac{2\delta_2(p,1) + \beta_2(p,1)}{4\alpha_2(p,1)\delta_2(p,1) + \gamma_2(p,1)\beta_2(p,1)}, \tag{3.5}$$

$$D_2(p) = \frac{SI}{2} \cdot \frac{\gamma_2(p,1) - 2\alpha_2(p,1)}{4\alpha_2(p,1)\delta_2(p,1) + \gamma_2(p,1)\beta_2(p,1)}, \tag{3.6}$$

and where

$$\gamma_n(p,r) = \left[p^2 + \frac{2n(n+1)}{r^2}\right] K_n(pr/c_1) + \frac{2p}{rc_1} K_{n-1}(pr/c_1) \quad \text{for } n = 0,2, \tag{3.7}$$

$$\alpha_2(p,r) = -2\left[\frac{3}{r^2}K_2(pr/c_1) + \frac{p}{rc_1}K_1(pr/c_1)\right], \tag{3.8}$$

$$\beta_2(p,r) = -\left\{\left[p^2 + \frac{12}{r^2}\right]K_2(pr) + \frac{2p}{r}K_1(pr)\right\}, \tag{3.9}$$

$$\delta_2(p,r) = -\frac{2}{r}\left[\frac{3}{r}K_2(pr) + pK_1(pr)\right], \tag{3.10}$$

and

$$I(p,t^*) \equiv I = \frac{1}{t^*p^2}(e^{-pt^*} - 1). \tag{3.11}$$

$K_n(z)$, $n = 0, 1, 2$, denotes the modified Bessel function of the second kind of order n.

The dynamic stresses may then be found by inverting the transformed equations (3.1)–(3.3). In order to obtain the complete solution the initial stress field must be added on.

For the present problem there are two wave speeds c_1, $c_2 = 1$ with $c_1 > c_2$, where c_1 is the speed of in-plane longitudiual waves and c_2 that of in-plane transverse waves. We then have four distinct circular wave fronts leaving the circular opening: two at $t = 0$ at the start of punching and two at t^* when punching stops. The fronts associated with c_1 have equations

$$r = 1 + c_1 t, \qquad r = 1 + c_1(t - t^*), \tag{3.12}$$

and those associated with c_2,

$$r = 1 + t, \qquad r = 1 + t - t^*. \tag{3.13}$$

We denote the fronts described by (3.12) as L_1, L_2 and those by (3.13) as T_1, T_2. At the opening the stresses σ_r, $\tau_{r\theta}$ unload linearly in time so that the boundary condition is continuous for all t but not differentiable at $t = 0$, t^*. As a result, since our problem is hyperbolic, the solutions have discontinuous derivatives at the four wave fronts and the graphs of the stress components as a function of time at a particular station, or along a ray at a fixed time, show corners at the fronts. Thus σ_r, σ_θ have corners propagating at speed c_1 and $\tau_{r\theta}$ at speed c_2. Ahead of the front $r = 1 + c_1 t$ all components retain their initial values. After all waves have passed, the solution decays to the static solution given by, for example, [3] as

$$\begin{aligned}
\sigma_r &= \frac{S}{2}\left[\left(1 - \frac{1}{r^2}\right) + \left(1 - \frac{4}{r^2} + \frac{3}{r^4}\right)\cos(2\theta)\right], \\
\sigma_\theta &= \frac{S}{2}\left[\left(1 + \frac{1}{r^2}\right) - \left(1 + \frac{3}{r^4}\right)\cos(2\theta)\right], \\
\tau_{r\theta} &= \frac{S}{2}\left(1 + \frac{2}{r^2} - \frac{3}{r^4}\right)\sin(2\theta).
\end{aligned} \tag{3.14}$$

We now turn our attention to describing the developing wave pattern. One way to do this is to introduce the isochromatric lines associated with the fringe patterns of photoelastic stress analysis. These are defined as the curves

$$\tau_{\max} = \text{constant}. \tag{3.15}$$

For our purposes we investigate the curves

$$\tau_{\max}/S = \text{constant} \tag{3.16}$$

at a sequence of time intervals. In order to do so we must invert (3.1)–(3.3) and insert the values in (3.16). This is intractable analytically and must be carried out numerically. We use the Fourier series approximation described in [4]. Once (3.1)–(3.3) have been inverted and the initial state added on, the stresses have the form

$$\begin{aligned}
\sigma_r/S &= f_1(r,t) + f_2(r,t)\cos(2\theta), \\
\sigma_\theta/S &= h_1(r,t) + h_2(r,t)\cos(2\theta), \\
\tau_{r\theta}/S &= g(r,t)\sin(2\theta).
\end{aligned} \tag{3.17}$$

The expression (3.16) may then be written as

$$A(r,t)\cos^2(2\theta) + 2B(r,t)\cos(2\theta) + C(r,t) = \left(\frac{2\tau_{\max}}{S}\right)^2, \tag{3.18}$$

where

$$\begin{aligned}
A(r,t) &= (f_2 - h_2)^2 - 4g^2, \\
B(r,t) &= (f_1 - h_1)(f_2 - h_2), \\
C(r,t) &= (f_1 - h_1)^2 + 4g^2.
\end{aligned} \tag{3.19}$$

Since our pattern is symmetric about both the x and y axes we concentrate on investigating the curves in the first quadrant.

Denote the roots of Eq. (3.18) by

$$X^{\pm}(r,t) = \left\{-B \pm \sqrt{B^2 - A\left[C - (2\tau_{\max}/S)^2\right]}\right\}/A, \tag{3.20}$$

with $X = \cos(2\theta)$, so that all curves of equal $\tau_{\max}$ in the first quadrant satisfy

$$\theta = \left(\cos^{-1}(X^{\pm})\right)/2. \tag{3.21}$$

Thus for a given time t and a choice of r, $1 \leqslant r \leqslant 1 + c_1 t$, (3.16) and (3.17) furnish the θ polar coordinate of a point on the curve (3.15).

4. Results. Once the polar coordinates r, θ of a given curve have been determined as described in Sec. 3, the graphs of curves of equal $\tau_{\max}$ are obtained for a sequence of values of t, and these are shown in Figs. 1 through 11. All results are for Poisson's ratio $\nu = 0.3$ and nondimensional punching time $t^* = 1.0$. This is a realistic value of t^* for plugging of an aluminum plate of thickness 0.5mm for normal impact by a cylindrical projectile of 11mm diameter travelling at 700 m/s. This point is discussed in detail in [5].

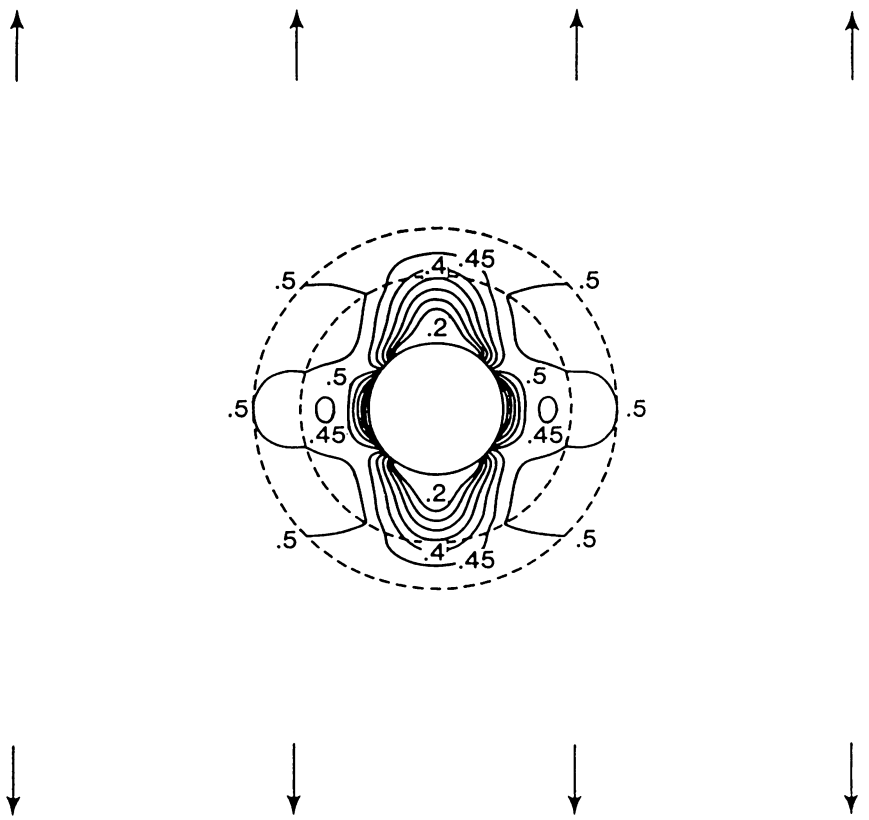

FIG. 1. Isochromatic lines at nondimensional time $t = 1$.

The dashed lines in the figures denote the four wave fronts L_1, L_2, T_1, T_2. In Fig. 1, since $t = t^* = 1$, only L_1 and T_1 are present; L_2 and T_2 are on the point of leaving the opening. The front L_2 is faster then T_1 and so catches it at time $t = c_1 t^*/(c_1 - 1)$. Thus for $t > 2.45$ both longitudinal fronts precede the transverse ones. For Figs. 7 to 11 the fronts have passed beyond the region shown in the diagram. As we pointed out, the r-derivatives of the stress components have finite jumps at the wave fronts so that curves of equal τ_{max} have corners there, and so the wave fronts are visible as the circular locus of these corners.

Figure 11 is computed directly from the well-known static solution given by Eq. (3.14). The sequence of figures display the evolution of the isochromatic curve pattern toward the static case. At $t = 15$, shown in Fig. 10, it is clear that the solution computed by the

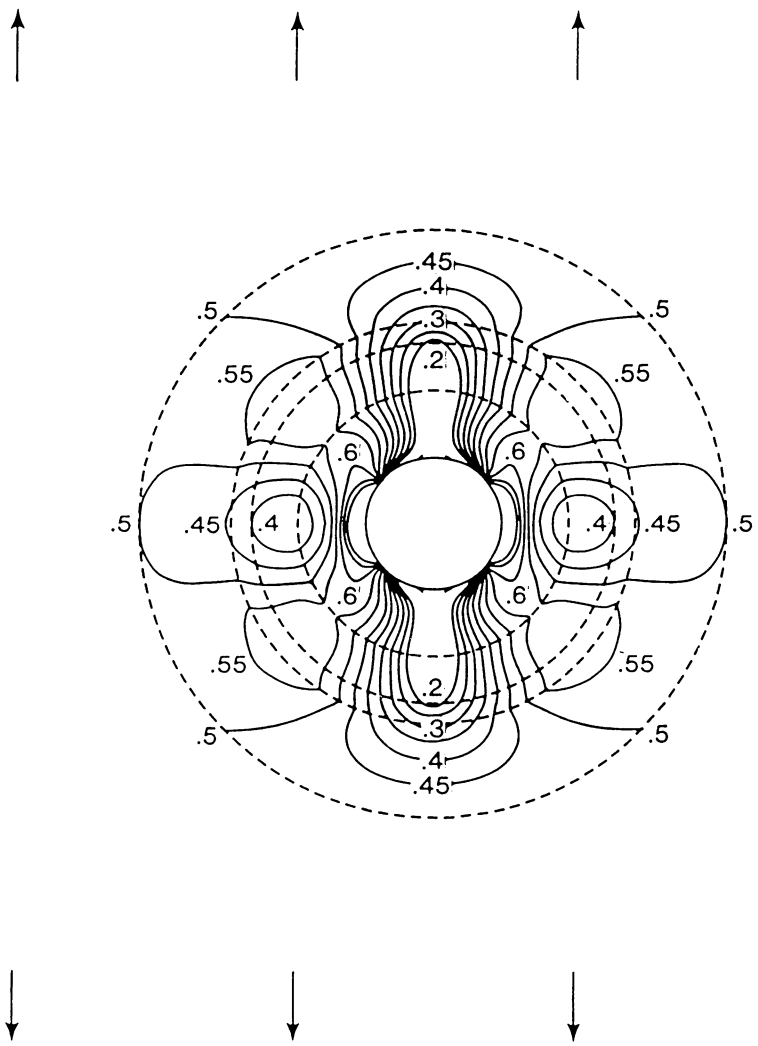

FIG. 2. Isochromatic lines at nondimensional time $t = 2$.

present method has essentially reached the static case for the region shown, that is, for $1 \leqslant r \leqslant 7$.

The curve $\tau_{max}/S = 0.5$ appearing in each figure is of particular interest since if $r > 1 + c_1 t$, we in fact have $\tau_{max}/S \equiv 0.5$. Thus this curve always intersects the leading wave front and for the static case stretches to infinity.

5. Conclusion. In the preceding paragraphs we have shown how the time-dependent isochromatic curve patterns may be computed and have supplied these patterns in the accompanying figures. The first advantage of such figures is in their contribution to visualizing how the stress pattern develops, how the wave fronts spread and interrupt the pattern, and where the stress concentrations are. The second advantage is in the connection between isochromatic lines and fringe patterns of photoelasticity. The final figure,

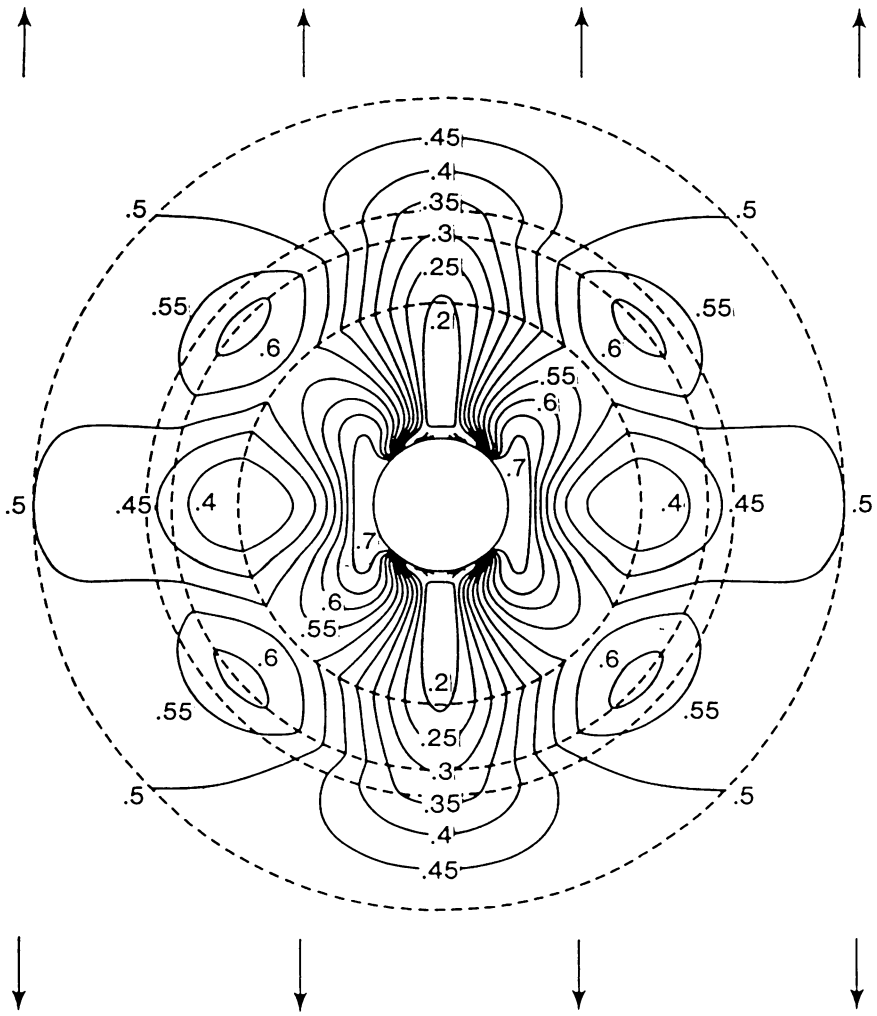

FIG. 3. Isochromatic lines at nondimensional time $t = 3$.

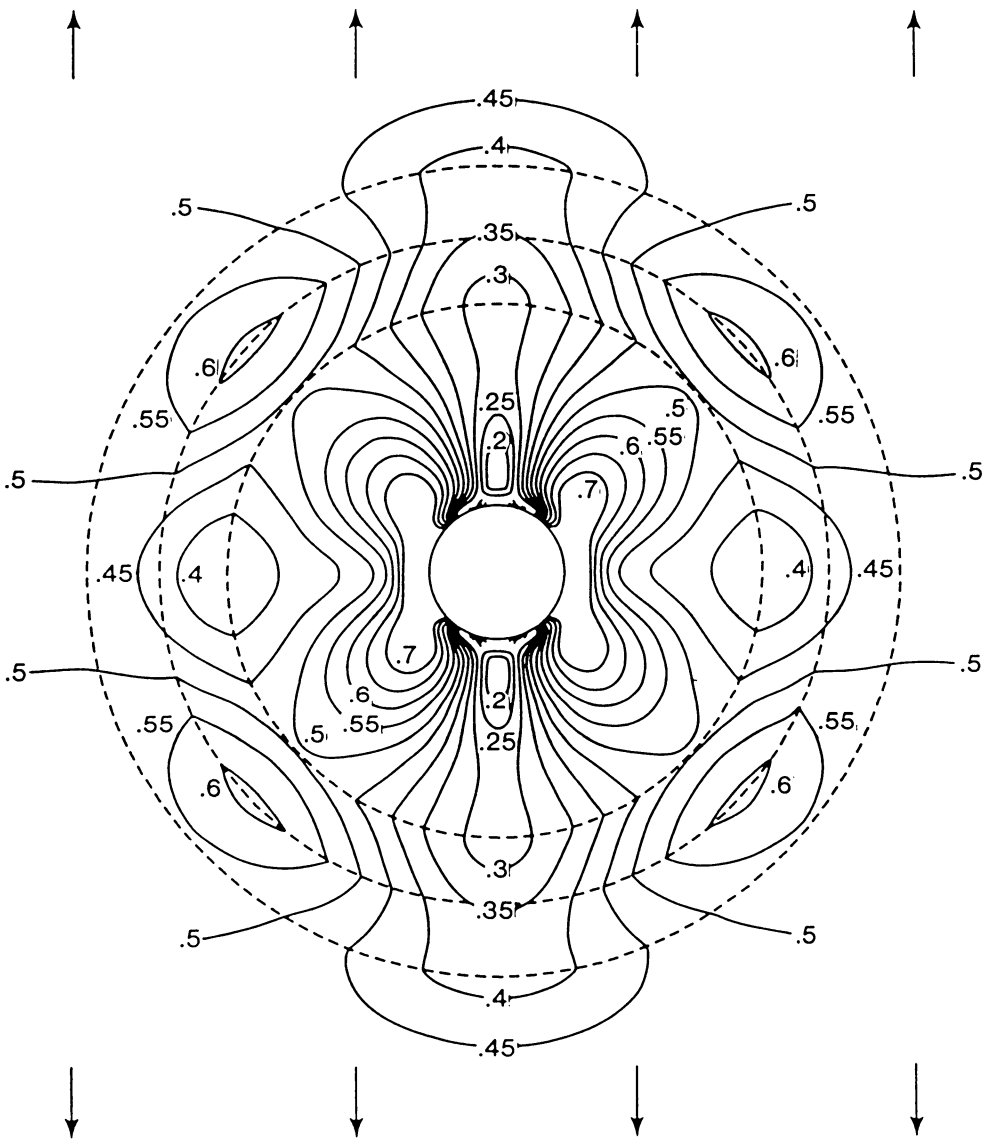

FIG. 4. Isochromatic lines at nondimensional time $t = 4$.

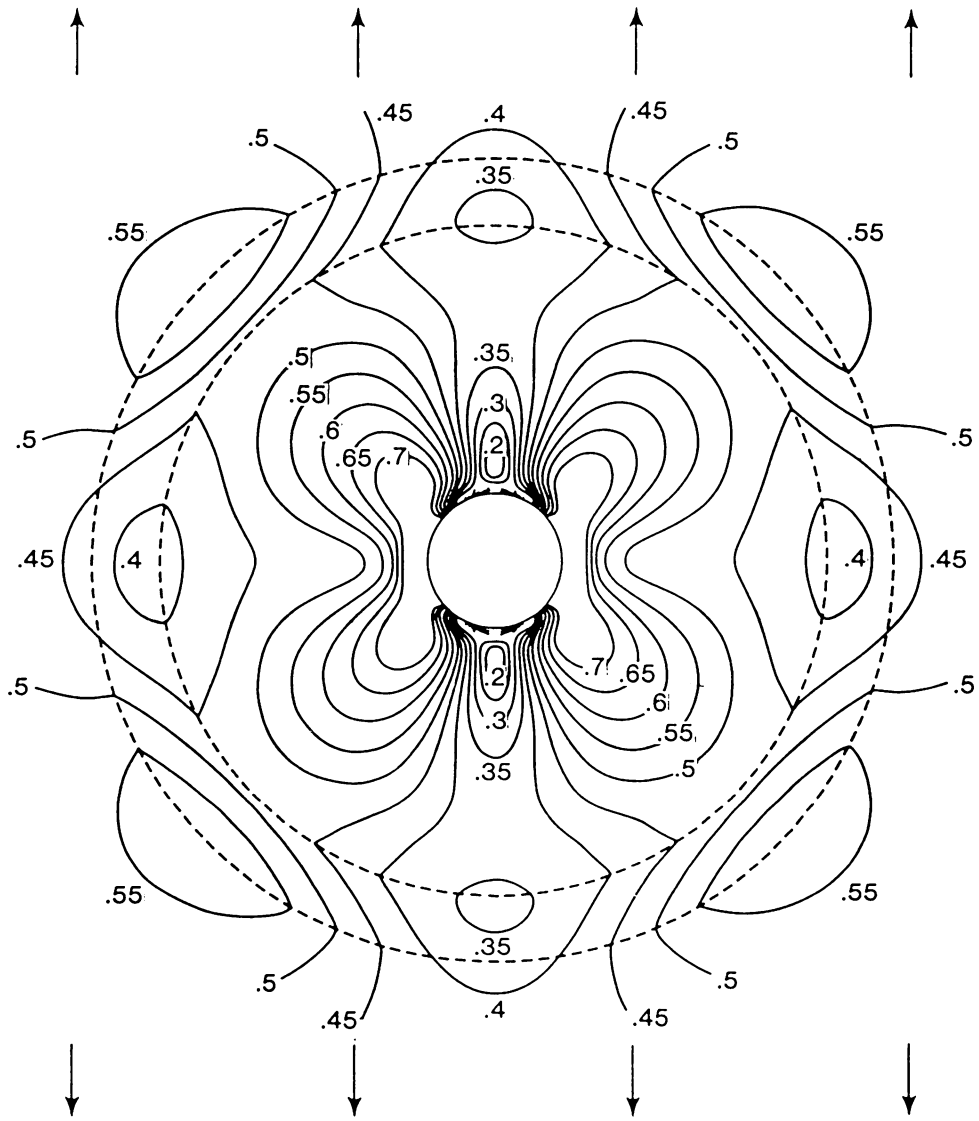

FIG. 5. Isochromatic lines at nondimensional time $t = 5$.

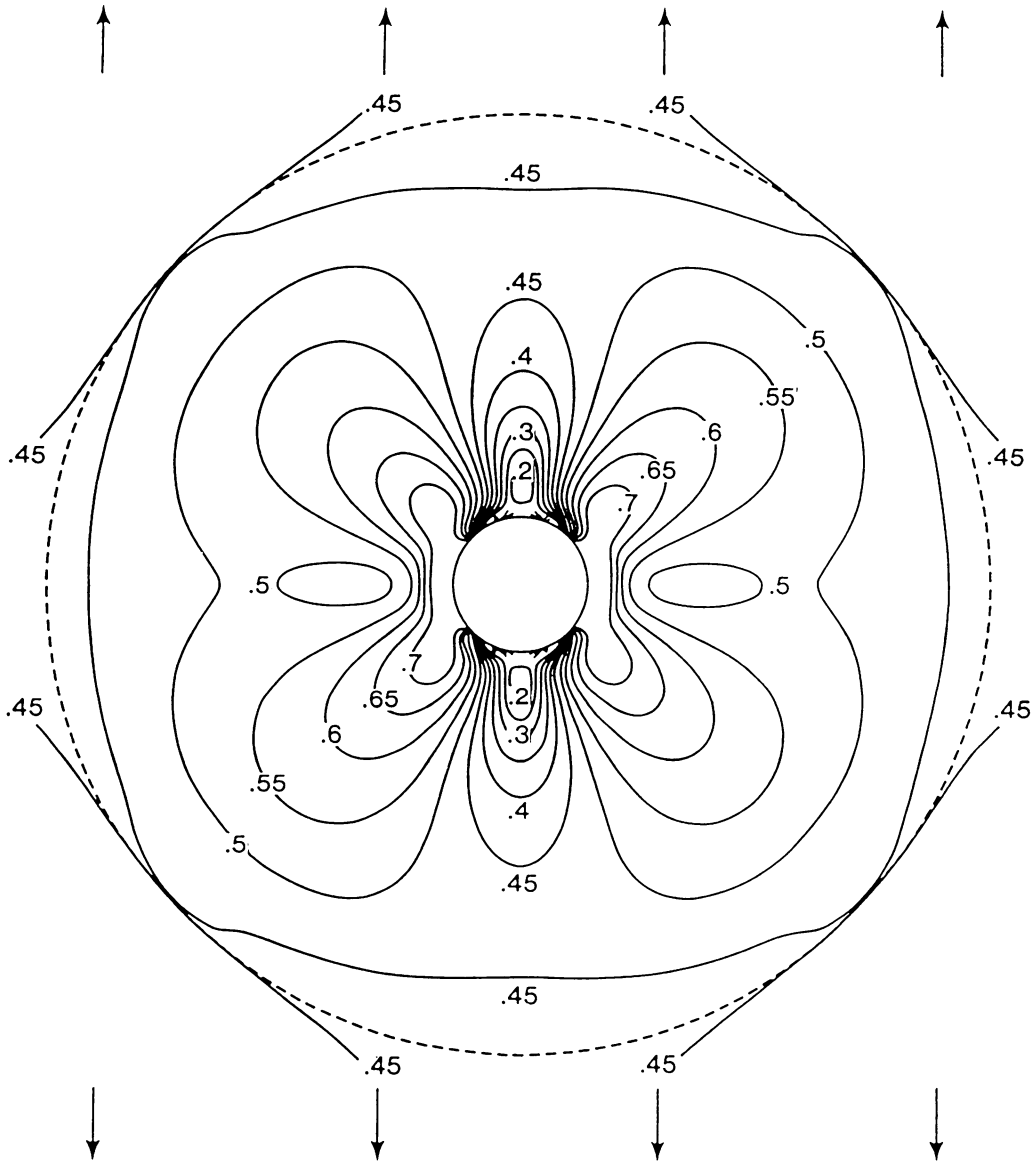

FIG. 6. Isochromatic lines at nondimensional time $t = 7$.

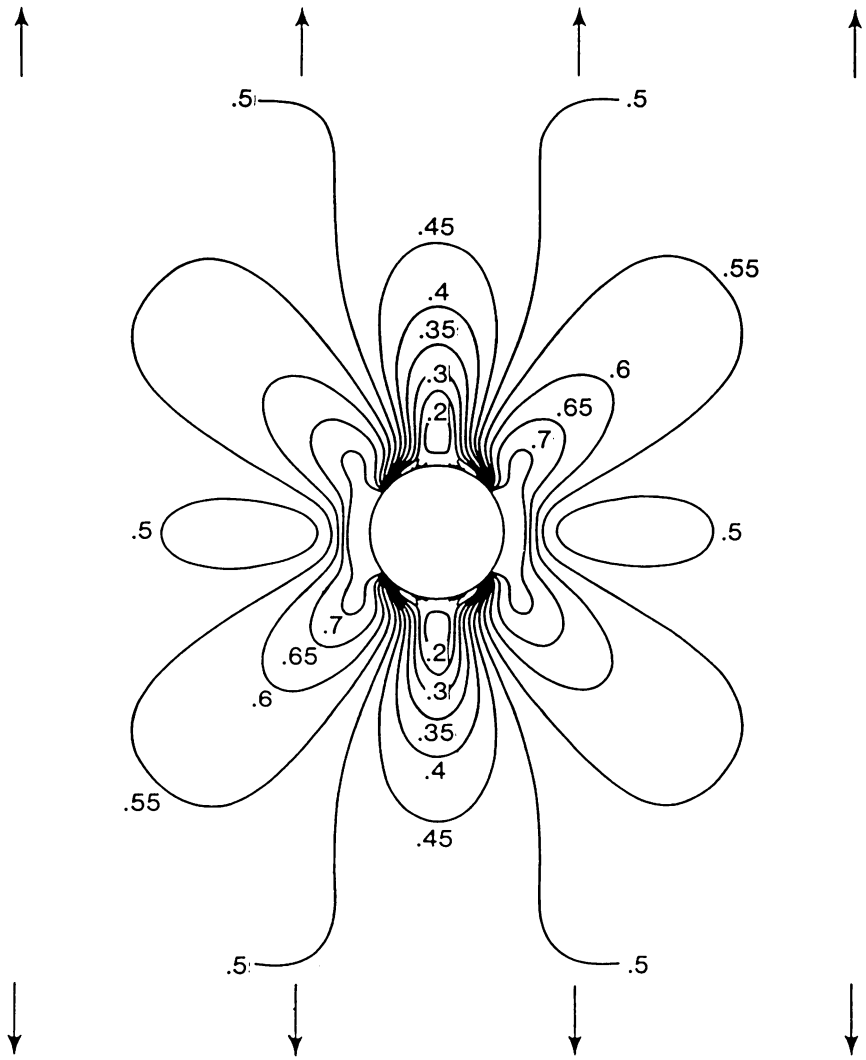

FIG. 7. Isochromatic lines at nondimensional time $t = 9$.

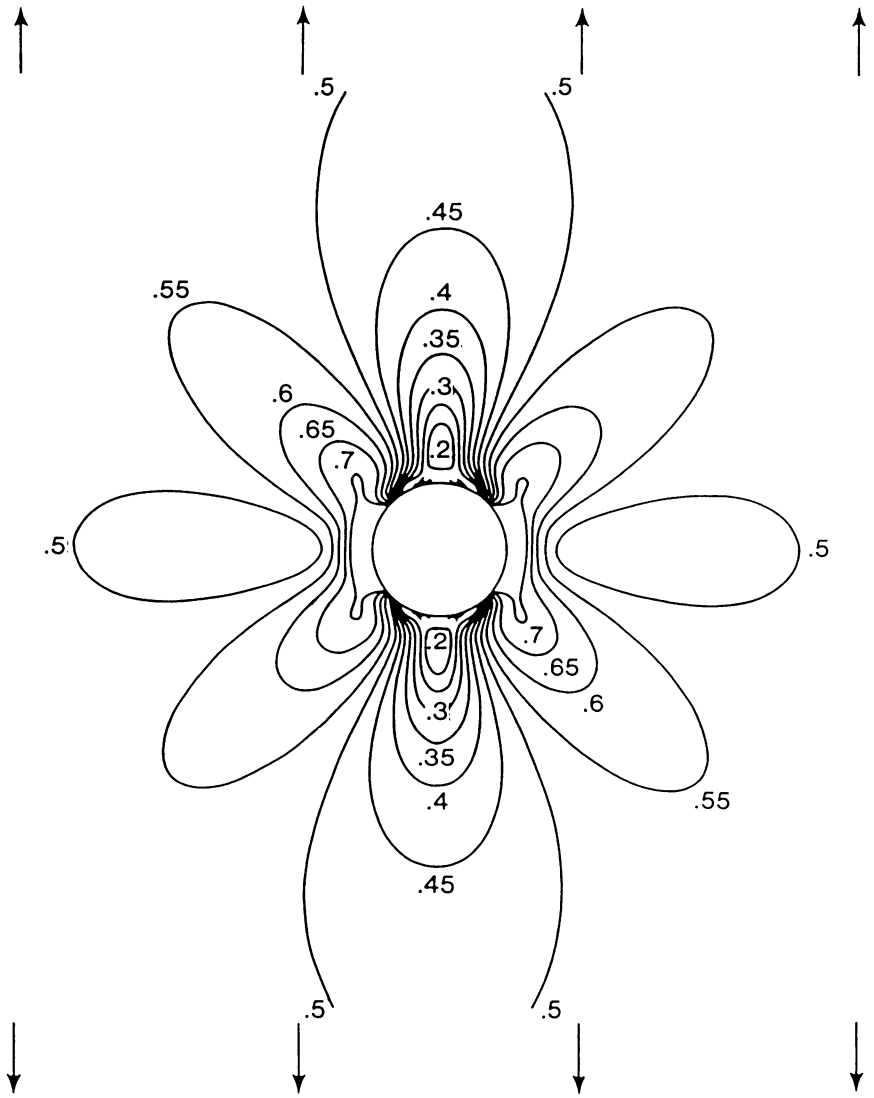

FIG. 8. Isochromatic lines at nondimensional time $t = 11$.

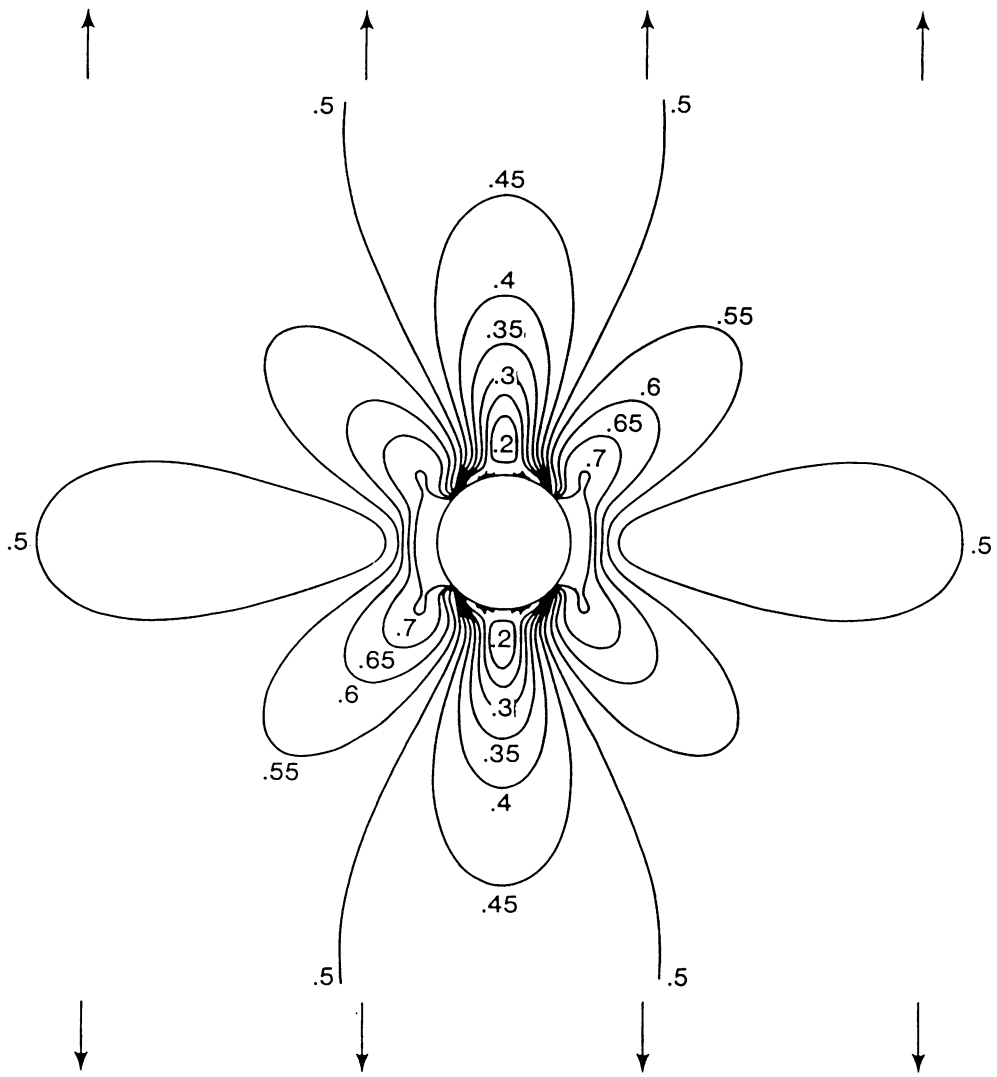

FIG. 9. Isochromatic lines at nondimensional time $t = 13$.

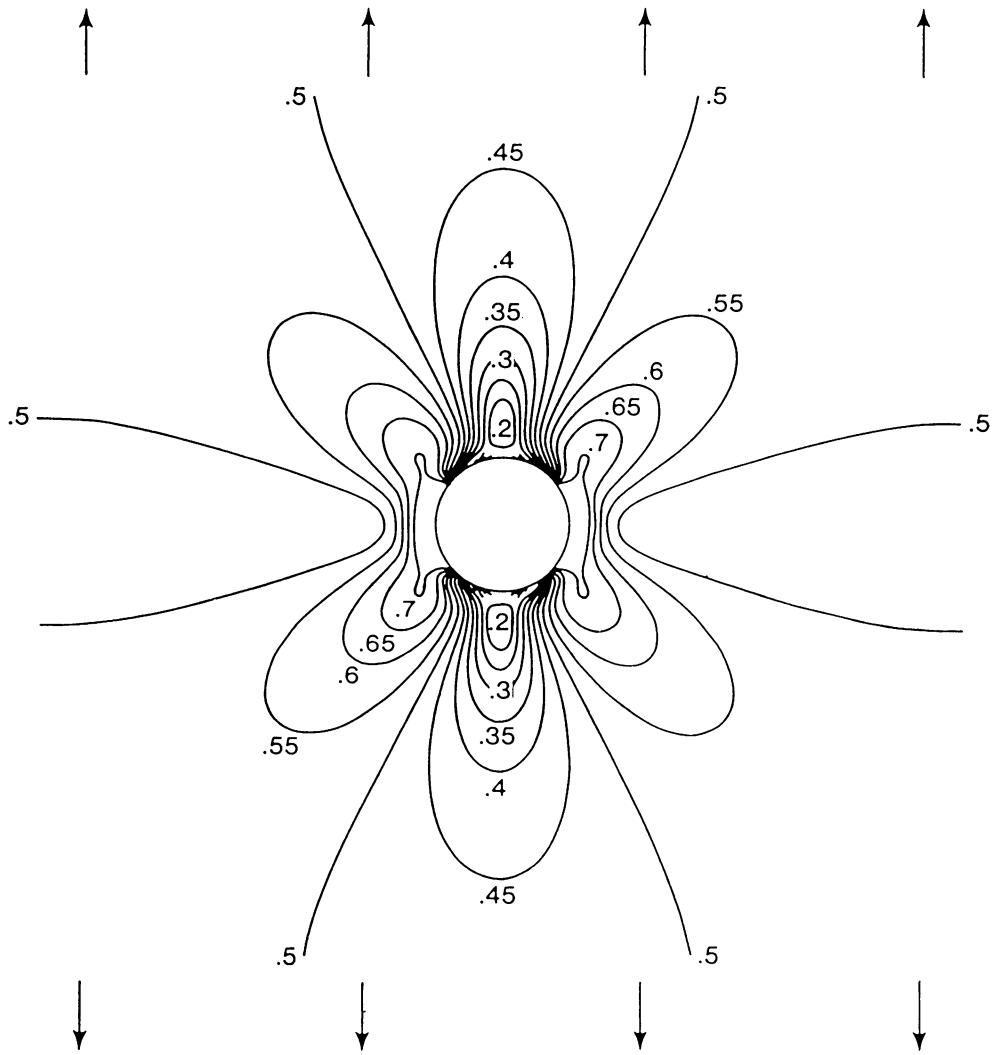

FIG. 10. Isochromatic lines at nondimensional time $t = 15$.

Fig. 11, is a well-known one and fringe patterns of this type are reproduced experimentally in, for example, [6]. This raises the possibility of reproducing the other diagrams experimentally, which would support the model we have used for plugging normal impact of a stretched plate.

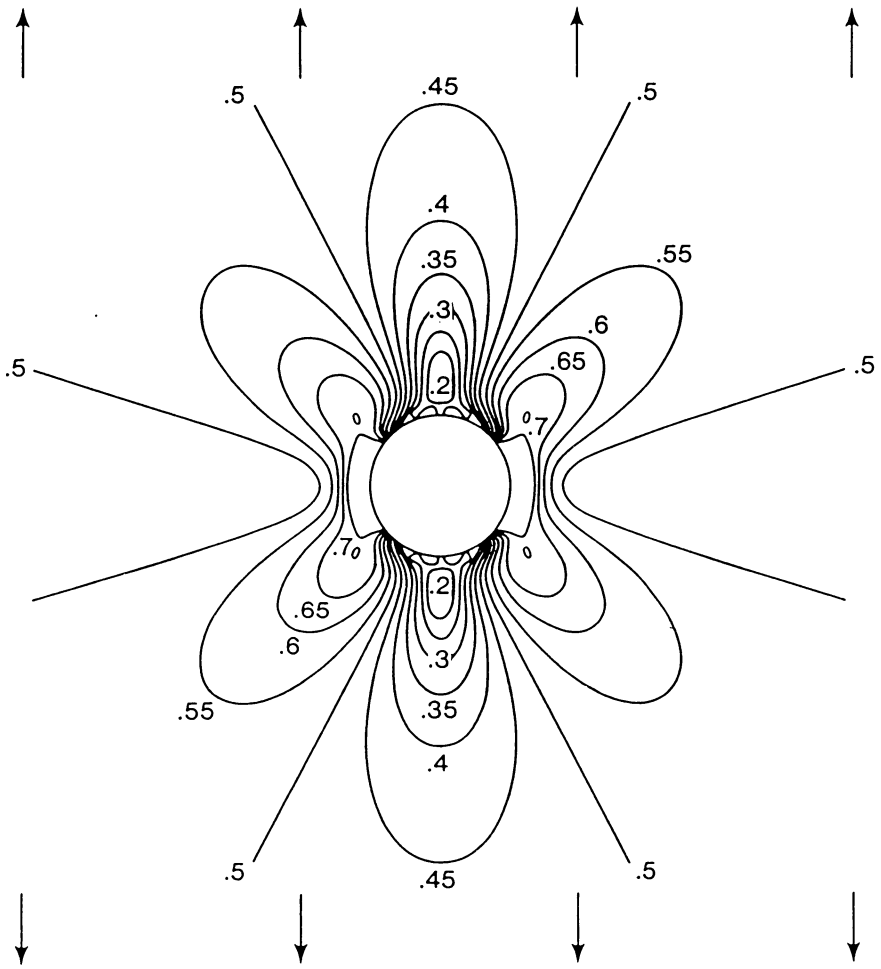

FIG. 11. Steady state situation, $t = \infty$.

References

[1] D. W. Barclay, T. B. Moodie, and J. B. Haddow, *Analysis of unloading waves from a suddenly punched hole in an axially loaded elastic plate*, Wave Motion **3** (No. 1), 105–113 (1981)

[2] J. Miklowitz, *Plane stress unloading waves emanating from a suddenly punched hole in a stretched elastic plate*, J. Appl. Mech. **27**, 165–171 (1960)

[3] G. N. Savin, *Stress concentration around holes*, Pergamon, New York, 1961

[4] K. S. Crump, *Numerical inversion of Laplace transforms using a Fourier series approximation*, J. Assoc. Comput. Mach. **23**, 89–96 (1976)

[5] J. B. Haddow and A. Mioduchowski, *Waves from suddenly punched hole in plate subjected to uniaxial tension field*, J. Appl. Mech. **46**, 873–877 (1979)

[6] E. Monch and R. Loreck, *Application of plane photoplastic experiments*, Symposium on photoelasticity (M. M. Frocht, ed.), Macmillan, New York, 1963